RSC Advances

ROYAL SOCIETY OF CHEMISTRY

www.rsc.org/advances

Osteogenic differentiation of adipose-derived stem cells in mesoporous SBA-16 and SBA-16 hydroxyapatite scaffolds

Gracielle F. Andrade[1,2], Juliana L. Carvalho[3], Armando S. C. Júnior [2], Alfredo M. Goes[3], Edésia M. B. Sousa[1]

[1]SENAN – Centro de Desenvolvimento da Tecnologia Nuclear - CDTN/CNEN

Av. Presidente Antônio Carlos, 6627 – Campus da UFMG – Belo Horizonte – MG

CEP 30270-901 - Brasil

[2] Faculdade de Farmácia – UFMG – Belo Horizonte – Brazil

[3]Instituto de Ciências Biológicas –Departamento de Bioquímica e Imunologia UFMG - Belo Horizonte – Brazil

KEYWORDS: Mesoporous silica, SBA-16, Hydroxyapatite, Osteogenic differentiation process.

ABSTRACT: Adipose-derived stem cells (ASCs) are currently a point of focus for bone tissue engineering applications. In this study, a biomaterial (HA-SBA-16) has been developed based on the growth of calcium phosphate (HA) particles within an organized silica structure (SBA-16) to evaluate their application in the osteogenic differentiation process. Indeed, pure SBA-16 was used to compare the effect of structural characteristics on the biological application. The samples were characterized by N_2 Adsorption, Transmission electron microscopy (TEM), Energy-dipersive X-ray spectroscopy (EDS) and Thermal analysis. *In vitro* assays were performed to evaluate the

viability, cytotoxicity and biological behavior of ASCs on SBA-16 and HA/SBA-16 nanocomposites to verify their potential as bioactive materials for application in bone-tissue engineering. The differentiation capacity of ASCs seeded in SBA-16 and HA/SBA-16 was confirmed by induction of the increase in AP production/activity of ASCs, expression of osteogenic gene markers (type I collagen mRNA, osteopotin and osteocalcin), and functionally, by Von Kossa staining. The results showed that those compositions have beneficial effects in stem cells, maintaining cell viability and allowing/promoting osteogenic differentiation.

INTRODUCTION

Materials used as medical implants are referred to as bioceramics, which are defined as ceramics for biorelated fields that are used in a number of different applications throughout the body [1]. The bioceramics field appeared in the late 1960s, as an effort to overcome some biocompatibility problems associated with the metallic implants used in orthopedics surgeries at that time.

Classified as bioceramics, calcium phosphate ceramics (hydroxyapatite) and silica-based bioactive glasses are the most representative components of this class of biomaterials[2]. Another common component of bioceramic materials is Hydroxy-carbonate apatite (HCA) which is chemically and structurally similar to the mineral phase in bone and thus provides a direct bonding by bridging host tissue with implants[1].

In addition mesoporous silica nanoparticles are also a well-studied class of ceramic systems. This extraordinarily diverse family of materials is mainly synthesized from one or two types of inorganic precursors, namely tetraalkoxysilanes and sodium silicate solutions. During mesoporous silica synthesis the pH of aqueous solution used enables control of hydrolysis and condensation

reaction rates needed to form ordered silicon dioxide matrices[3]. The silica matrix is non-crystalline and contains abundant surface silanol groups, which offer a cytocompatible interface.

The SBA-type silica materials (*Santa Barbara*) attract attention by exhibiting high surface areas, thick pore walls, high pore volumes and narrow pore size distribution. The synthesis of a variety of mesoporous SBA-type silica materials using non-ionic triblock copolymers as templates was reported by Zhao and co-workers[4,5]. Among the SBA-type silica materials developed so far, SBA-16 (*Santa Barbara Amorphous number* 16) is considered to be the most interesting mesostructure, as it contains pore sizes of approximately 5 to 15 nm, with a 3D cubic arrangement of mesopores[6]. They act as a convenient reservoir for enclose guests due to their large pores, high hydrothermal stability and easy preparation, constituting promising materials for a large range of applications, especially as biomaterials, due to their spherical morphology[7]. Another interesting feature of this class of materials is that the presence of silanol groups in the external surface of silica walls would allow the growth of apatite layers.

Bioactive ceramics bind to and integrate with living bone in the body without forming fibrous tissue around them[8]. Also, some bioglass compositions can promote the activation of genes that stimulate the regeneration of bone tissues [2,9].

The generation of sol-gel mesoporous glasses for biomedical applications exhibit better bioactivity behaviour due to their outstanding values of surface area and porosity, as well as capability to host active agents that contribute to the tissue's healing processes. These materials combined with hydroxyapatite obtained by a sol-gel process have demonstrated excellent bioactivity [10]. Additionally, the release of calcium and silicon ions may be contributing to the modulation of

cellular attachment by promoting of the control the cell cycle of osteoprogenitor cells [11]. Thus, the biomaterial can be serving as a guiding structure for initial tissue development.

In order to be used in their full potential and to consolidate their application as tissue engineered constructs, bioceramic materials can be associated with stem cells and their differentiation-derived cell types, such as osteoblasts. As a multidisciplinary field, tissue engineering combines cells, scaffolds and growth and differentiation factors with the purpose to develop biological substitutes for the restoration, maintenance or improvement of tissue function [12].

In the present study, we propose to study two different bioceramic materials, namely SBA-16 and HA/SBA-16, according to their biomechanical and stability properties. Since the data generated here is indicative of two compositions with very interesting properties, such as porosity and stability, we continued our work by evaluating cytocompatibility and biological effects of those compositions using stem cells. We finish concluding that those compositions have beneficial effects in stem cells, maintaining cell viability and allowing/promoting osteogenic differentiation.

EXPERIMENTAL SECTION

Materials

Tetraethyl-orthosilicate (TEOS), 3-amino-propyltriethoxysilane (APTES), Fetal Bovine Serum (FBS), Penicillin, Streptomycin, Amphotericin B, b-glycerophosphate, isobutylmethylxanthine, indomethacin Collagenase I, Sodium Bicarbonate and Dulbecco's modified Eagle's medium (DMEM) were purchased from Sigma Aldrich (St. Louis, MO, USA). Gentamicin was obtained from Schering-Plough), Fetal Bovine Serum from Cripion Biotecnologia LTDA, Brazil. Dexamethasone from Aché, insulin from Eli Lilly and Company, Ascorbate-2-phosphate from Ecibra, Trypsin-EDTA from Gibco, USA. 3-(4,5-dimethiol-2-thioazolyl)-2,5-diphenyl tetrazolium

bromide (MTT), $(NH_4)_2HPO_4$ and Pluronic F127 (Mav=12600) were purchased from Sigma Aldrich (São-Paulo-Brazil). PBS, Trizol reagent and 5-Bromo-4-chloro-3-Indolyl phosphate (BCIP)/Nitroblue tetrazolium salt (NBT) Kit assay from Invitrogen, SP, Brazil). $AgNO_3$ was obtained from Vetec, $Na_2S_2O_3$ from Cinética Química, Xilol and $Ca(NO_3)_2.4H_2O$ from Labsynth, Brasil.

Synthesis of Mesoporous Silica SBA-16

Silica-block copolymer mesophases were synthesized using Pluronic F127 (poly (ethylene oxide)-block-poly (propylene oxide)-block-poly (ethylene oxide)), M_{av}=12600, as a templating agent at room temperature. In a preparation, 3.0 g of Pluronic F127 was dissolved in 144mL of water and 13.9 mL of 38% HCl solution under constant stirring at 25°C. After approximately 30 minutes, 11mL of co-surfactant butanol was added to reach a 1:3 (F127:BuOH) mass ratio in the ternary system. Next, 15.3 mL of tetraethyl orthosilicate (TEOS, Sigma-Aldrich) was added to the solution under constant stirring at 45°C for 1 h, according to the method reported by Gobin[13]. After aging at 100°C for 24 h in a hermetically closed recipient, the solids were collected by filtration and dried in open air at 37°C. The surfactant was removed by calcination, which was carried out by increasing the temperature to 550°C under nitrogen flow for 5 hours at a rate of 5°C/min. Chemical analysis showed that the surfactant had been completely removed by this thermal treatment.

Synthesis of HA/SBA-16 Composite

The synthesis of the material has been carried out using a two-step procedure, which is detailed as follows:

Preparation of the Ca-doped Silica Matrix

The first step (low pH step) consisted of the preparation of a calcium doped silica matrix that was obtained by means of a variation of the methodology described by Andrade *et. al.*[10]. Silica-block copolymer mesophase SBA-16/HA composites were synthesized using Pluronic F127 (poly(ethylene-oxide)-block-poly(propylene-oxide)block-poly(ethylene-oxide), M_{av}=12600, as a structure reacting agent, which was reached at room temperature. In a typical preparation, 3.0 g of Pluronic F127 was dissolved in 200 mL of $Ca(NO_3)_2$ solution and 100 mL of HCl 2M solution with constant stirring at 25°C. After approximately 30 min, 11 mL of the cosurfactant butanol was added to reach a 1:3 (F127:BuOH) mass ratio in the ternary system. Next, 15.3 mL of tetraethyl orthosilicate (TEOS, Sigma-Aldrich) was added to the solution, under vigorous stirring at 45°C for 1 h, according to the method reported by Gobin[13], and then aged at 100°C for 24 h in a hermetically closed recipient. Next, the product was dried in an oven at 100°C.

HA Crystallization Within the Ca-doped Matrix

In the second step (high pH step), the Ca-doped silica was dropped into a $(NH_4)_2HPO_4$ solution, and the pH values were adjusted to 9. After, the solution was submitted to a second hydrothermal treatment at 100°C for 24 h. The powder was then washed and heat-treated in open air at 600°C for 6 hours to obtain the final (HA/SBA-16) material[14].

Physicochemical and Morphological Characterization of SBA-16 and HA/SBA-16

All samples of SBA-16 and HA/SBA-16 composite were physicochemically characterized by N_2 adsorption, Energy-dipersive X-ray spectroscopy (EDS), Transmission electron microscopy (TEM) techniques and Thermogravimetric analyses (TGA). Nitrogen adsorption isotherms of samples were obtained at 77 K using a Quantachrome SiQwin™- Automated Gas Sorption Data

adsorption analyzer. Before the adsorption measurements, SBA-16 and HA-SBA-16 composites were outgassed for 2 h at 120°C. All data analyses were performed using the NovaWin, 1994–2011 Quantachrome Instruments software (Boynton Beach, FL, USA). The matrices were dispersed in deionized water and were sonicated in ultrasonic bath for 5 minutes. After that, the morphological characteristics and internal porous structure of SBA-16 and HA/SBA-16 were studied by using the TEM technique. TEM images were captured on a Tecnai G2 – Spirit – FEI-2006, using an accelerating voltage of 120kV, with magnification of 100.000x and the iTEM software manufactured by AnalySis. Transmission electron microscopy has associated an energy-dispersive X-ray spectrometer where EDS measures was performed during the image capture. TGA was carried out on a TGA 50WS (Schimadzu) thermal analyzer with the speed of heating as 5°C.min^{-1} and the temperature ranging from 25-800°C under nitrogen atmosphere.

Basal Cell Culture Medium

Dulbecco's Modified Eagle's Medium–high glucose (DMEM) was supplemented with 3,7 g/L Sodium Bicarbonate, Penicillin (100 U/mL), Streptomycin (0.1 mg/mL), Amphotericin B (0.25 mg/mL), Gentamicin (60 mg/L), and 10% v/v Fetal Bovine Serum (FBS).

Osteogenic Medium

Osteogenic medium (OM) consisted of basal medium (BM) supplemented with 50 μg/mL ascorbate-2-phosphate, 10 mM b-glycerophosphate and 0.1 μM dexamethasone [15].

Adipogenic Medium

Adipogenic medium consisted of BM supplemented with 0.5 mM isobutylmethylxanthine, 200

μM indomethacin, 1 μM dexamethasone, and 10 μM insulin [16]. The adipogenic induction medium was changed every two days.

Chondrogenic Medium

The induction of chondrogenic differentiation was carried out in a three-dimensional pellet culture using the StemPro Chondrogenesis Differentiation Kit.

ASC Isolation and Culture

ASCs were isolated from gonadal adipose tissue depots from male Lewis rats 6-8 weeks old, as previously described[17,18]. All experimental protocols were performed in accordance with the guidelines for the humane use of laboratory animals established at our Institution. This study was approved by the Committee of Ethics in Research at the Federal University of Minas Gerais (Protocol #61/2010). The protocol was adapted from[16,19]. After euthanasia, animals were washed with 70% ethanol and placed in a laminar flow hood. An incision was made in the Linea Alba to expose the peritoneum and allow gonadal adipose tissue depots isolation. The collected material was washed in phosphate-buffered saline (PBS), minced and digested with 0.15% collagenase I for 1 h. After digestion, collagenase I activity was inhibited by the addition of Basal medium. The material was spun at 1500 rpm for 10 minutes, the supernatant removed and the pellet resuspended in BM. Cells were plated in 75 cm^2 culture flasks and maintained in a 5% CO_2 incubator at 37ºC for 24h before first media change. Following, media was changed every 2-3 days. At 80–90% confluence, cells were detached using 0.05% trypsin-EDTA and replated in other flasks at 1:3 ratios. Third passage ASCs were used in all experiments.

Adipogenic Differentiation and Oil Red Staining

For adipogenic differentiation, MSCs at passage 3 were seeded at 500 cells/cm^2 in 6-well plates

and cultured in adipogenic medium. After 21 days, cells were washed with PBS, fixed in 10% formalin for 60 min, followed by a wash with 60% isopropanol. The cells were stained with an Oil-Red O (Thermo Scientific) solution in 60% isopropanol for 5 min, rinsed with deionized water, and counterstained with hematoxylin for 1 min.

Chondrogenic Differentiation and Alcian Blue Staining

For chondrogenic differentiation, 5×10^5 cells were centrifuged at 800 g for 5 min in a 15-ml polypropylene conical tube (Sarstedt). Pellets were then cultured for 21 days in chondrogenic medium, which was changed twice a week. Differentiation was assessed by proteoglycan and glycosaminoglycan staining of formalin fixed, paraffin embedded, 5 μm sections of the pellets with Alcian Blue 8GX (1% in acetic acid, pH 2.5) for 30 min and counterstaining with hematoxylin for 1 min[20].

Flow Cytometry Analysis of ASC Phenotypic Profile

Immunophenotypic analysis was performed with 3rd passage ASC as previously described[15,18]. Briefly, cells were detached from cell culture surface and counted. One million cells were washed and incubated with one of the primary unconjugated antibodies for 30 min at 4°C (Table 1). Following incubation, cells were washed with PBS and incubated with secondary antibodies for another 30 min at 4°C. Flow cytometry was performed using a Guava® easyCyte™ 6-2L Flow Cytometer (Millipore). Five thousand events were acquired using the software Incyte (Millipore) and analyzed using FlowJo 7.5.6.

Table 1. List of antibodies used in flow cytometry

Antibody reacts with	Supplier	Catalog Number	Dilution
CD11 b/c	BD Pharmingen	554859	1:50
CD34	Santa Cruz Biotech. Inc.	Sc-7324	1:50
CD45	BD Pharmingen	610266	1:50
CD54	BD Pharmingen	554967	1:50
CD73	BD Pharmingen	551123	1:50
CD90	BD Pharmingen	554892	1:50
RT1A	BD Pharmingen	554917	1:50
I-Ad/I-Ed	BD Pharmingen	558593	1:50
Goat anti Mouse IgG Alexa-Fluor 488	Molecular Probes – Invitrogen	A-11001	1:200

Cell Seeding

Cell seeding started by detaching cells from culture surface and counting. Five thousand cells/well were seeded in 24 well plates (Sarstedt, Nümbrecht, Germany) for viability/cytotoxicity, alkaline phosphatase production assays. Fifty thousand cells were seeded in 6 well plates (Sarstedt, Nümbrecht, Germany) for gene expression and ECM mineralization assessment. Cells were allowed to attach for 1 hour in a humidified atmosphere at 37°C and 5% CO_2, when SBA-16 and HA/SBA-16 biomaterials were added to the wells. Cells were seeded in BM or OM, according to each group.

In vitro Cytotoxicity During Differentiation

Viability and cytotoxicity of ASC cultured in the presence of SBA-16 and HA/SBA-16 were assessed by the tetrazolium salt MTT (3-[4,5-dimethylthiazol-2-yl]-2, 5-diphenyltetrazolium bromide) assay, which is based on the reduction of tetrazolium salt to formazan crystals by the dehydrogenases present in living cells mitochondria and other cell compartments[21]. The assay was performed at various culture times, namely 1, 7, 14 and 21 days after cell seeding. First, medium was removed and 210 µl of fresh BM and 170 µl of MTT solution at 5 mg/mL diluted in PBS (Invitrogen, São Paulo, SP, Brazil) were added to each well. Cells were then incubated for 2 h in a humidified atmosphere at 37°C and 5% CO_2. The resulting formazan crystals were dissolved by addition of 210 µl of sodium dodecyl sulfate (SDS)-10% HCl solution. After 18 h, 100 µl of solution was transferred to 96-well plates, and the optical density (OD) was measured at 595 nm. Biomaterials without cells were subjected to the same procedure, as a control.

Alkalyne Phosphatase Production Analysis

Alkalyne Phosphatase (AP) production was assessed with the 5-Bromo-4-chloro-3-Indolyl phosphate (BCIP)/Nitroblue tetrazolium salt (NBT) Kit assay, following manufacturer's instructions. Briefly, at days 1, 7, 14 and 21, cells were washed with PBS and 200 µl of BCIP/NBT solution were added to each well. After 2 h in a humidified atmosphere at 37°C and 5% CO_2, insoluble purple precipitants were dissolved with SDS-10% HCl solution. After 18 h, 100 µl of solution was transferred to a 96-well plate and the OD was measured at 595nm. Again, biomaterials alone were subjected to the same procedure, as a control.

Reverse Transcriptase–Polymerase Chain Reaction

Osteocalcin (OC), Osteopontin (OP) and Collagen I (COL I) expression was evaluated at mRNA level with Reverse Transcriptase-Polymerase Chain Reaction (RT-PCR) at 21 days of culture. Groups included cells cultured in BM and OM in the presence or absence of SBA-16 or HA/SBA-16.

Initially, total RNA was isolated using Trizol reagent (Invitrogen, São Paulo, SP, Brazil) following manufacturer instructions. RNA concentration was determined using NanoDrop ND-1000 Microspectrophotometer and 1 μg of total RNA of each sample was treated with the RevertAidTM H Minus M-MuLV RT (Fermentas) to generate cDNA using an oligo(dT) adapter primer. Then, Glyceraldehyde 3-phosphate dehydrogenase (GAPDH) amplification was performed in order to assess cDNA quality, followed by OC, OP and COL I amplification (Table 2). The RT-PCR products were analyzed through 1% agarose gel electrophoresis and visualized with ethidium bromide.

Table 2. Primer information

Primer	Sequence (5' – 3')	Amplicon (bp)	Tm (°C)
GAPDH F	TGCCACCACCAACTGCTTA	177	60
GAPDH R	GGATGCAGGGATGATGTTC		
Osteopontin F	GGATGAACCAAGCGTGGAAACAC	212	59
Osteopontin R	CCTCATGGCTGTGAAACTCGTG		
Osteocalcin F	AGCCTTCATGTCCAAGCAGGAG	205	59
Osteocalcin R	CTAAACGGTGGTGCCATAGATGC		
Collagen I F	ACTGCAACATGGAGACAGGTCAG	257	59
Collagen R	GGCTACGCTGTTCTTGCAAGTGAT		

Von Kossa Staining

Functional assessment of osteogenic differentiation was performed by evaluation of mineralization of extracellular matrix (ECM), it was assessed performing Von Kossa staining. Briefly, cells were rinsed with distilled water and fixed in 70% ethanol for 24 h. Following incubation, cells were kept in 5% w/v $AgNO_3$ solution for 2 h in a dark chamber containing one incandescent light source. Cells were washed again and incubated in 5% w/v $Na_2S_2O_3$ solution for 5 minutes and counterstained with eosin. Finally, cells were dehydrated and cleaned with xilol. Secretion of calcified extracellular matrix was confirmed as black nodules with Von Kossa staining.

Statistical Analysis

All experiments were repeated three times with triplicate samples. Statistical analysis were

performed by using Graph Pad Prism 5.0. The values were represented as the mean – standard deviation. Statistical differences were calculated by using analysis of variance and Bonferroni's post-tests. Differences were considered significant at $p<0.05$.

RESULTS

N_2 Adsorption

An assessment of the porosity of the reference SBA-16 and the HA/SBA-16 materials was performed using N_2 adsorption/desorption isotherms (Figure 1). Both samples exhibit a type IV isotherm characteristic of mesoporous materials. Note that the form of the hysteresis loop is affected by the incorporation of hydroxyapatite within the silica sample. The SBA-16 material shows the H2-type hysteresis loop characteristic of mesoporous materials with three-dimensional cubic channels. HA/SBA-16 shows a H3-type hysteresis loop, which is often observed with aggregates of plate-like particles, which in turn give rise to slit-shaped pores[14]. Another observation from this data is that HA incorporation leads to significant decreases in the amount of adsorbed nitrogen, thus provoking other changes in structural characteristics. As can be observed (Table 3), this result reveals the decrease in pore volume and shows that the presence of HA in the SBA-16 matrix leads to a significant decrease in the surface area. This result indicates that HA growth crystals block the available spaces of the mesoporous silica and are responsible for increasing the average pore size diameter[22]. According to Shi [23], the pores within the mesopore range can act as initiation sites for HA crystal nucleation, suggesting that increasing levels of calcium and phosphate ions inside the pores promoted the precipitation of HA within this region. The P/P_0 position of the inflection range from 0.40 to 0.80, which is characteristic of capillary condensation, confirms this structural pore characteristic, and the sharpness of the step indicates the uniformity of the mesopore size distribution. Furthermore, the nitrogen adsorption technique

yields information about the presence of micropores which are characteristic of the 3D material corresponding to spaces between the interconnecting pores, as presented in Table 3.

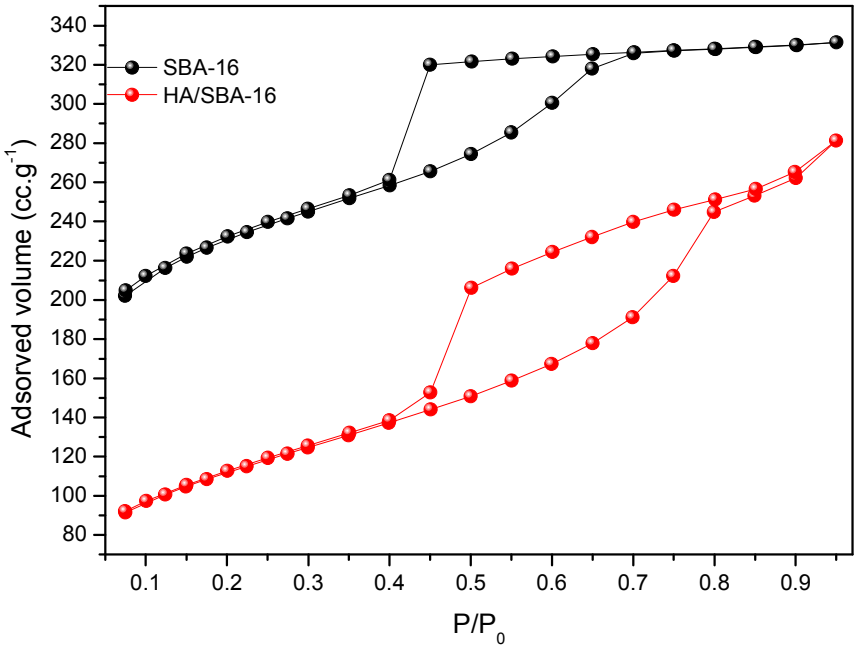

Figure 1: Nitrogen adsorption isotherms.

Table 3. N_2 adsorption of SBA-16 and HA/SBA-16 samples.

Samples	D_p (nm)	S_{BET} ($m^2.g^{-1}$)	S_{micro}($m^2.g^{-1}$)	V_p ($cc^3.g^{-1}$)	V_{micro}($cc^3.g^{-1}$)
SBA-16	3.4	735	413	0.244	0.117
HA/SBA-16	3.8	384	90	0.351	0.046

Notation: D_p, pore diameter defined as a maximum on the pore size distribution, S_{BET}, BET specific surface area, S_{micro}, surface area from micropores from t-plot method, V_P, total pore volume calculated at relative pressure P/P_0 0.98, V_p and V_{micro} are the average pore volume and micropore volume evaluated using the α_s-plot method, respectively. N_2 adsorption error: 3%

Transmission Electron Microscopy (TEM) and Energy-Dispersive X-ray Spectrocopy (EDS)

The TEM images of the parent SBA-16 silica are shown (Figure 2). These images presented a cubic array of uniform channels when the incident electron beam was parallel to the main axis of the mesopores, and unidirectional channels when the electron was perpendicular to the channel axis. The unit cell parameter was approximately (15.2 ± 0.7) nm, which is in agreement with the SAXS data that was previously published by Andrade et.al. [10]. The TEM images from HA/SBA-16 materials (Figure 2) showed no significant difference in the spacing between channels from one of the parent SBA-16 silica, thus proving that the ordered structure is preserved in the approach proposed in the present work to obtain a nanocomposite mesoporous material. It could be noticed (Figure 2) that the image displayed many separate hydroxyapatite nanocrystals dispersed around the SBA-16 matrix, which proves the hydroxyapatite formation. One HA/SBA-16 image showed the presence of hydroxyapatite crystals within the silica pores. This image confirms the possibility of the porous blocking of the material for that crystal. These results are agreement with that obtained by N_2 adsorption-desorption isotherms and BJH pore size distribution curves for HA/SBA-16. The HA/SBA-16 presents smaller surface areas than do pure SBA-16 materials, and the pore sizes of HA/SBA-16 were larger than those of SBA-16. The assembled HA and its subsequent growth within the pores of SBA-16 may well decrease the surface area of mesoporous materials as well as increase the pore size [23].

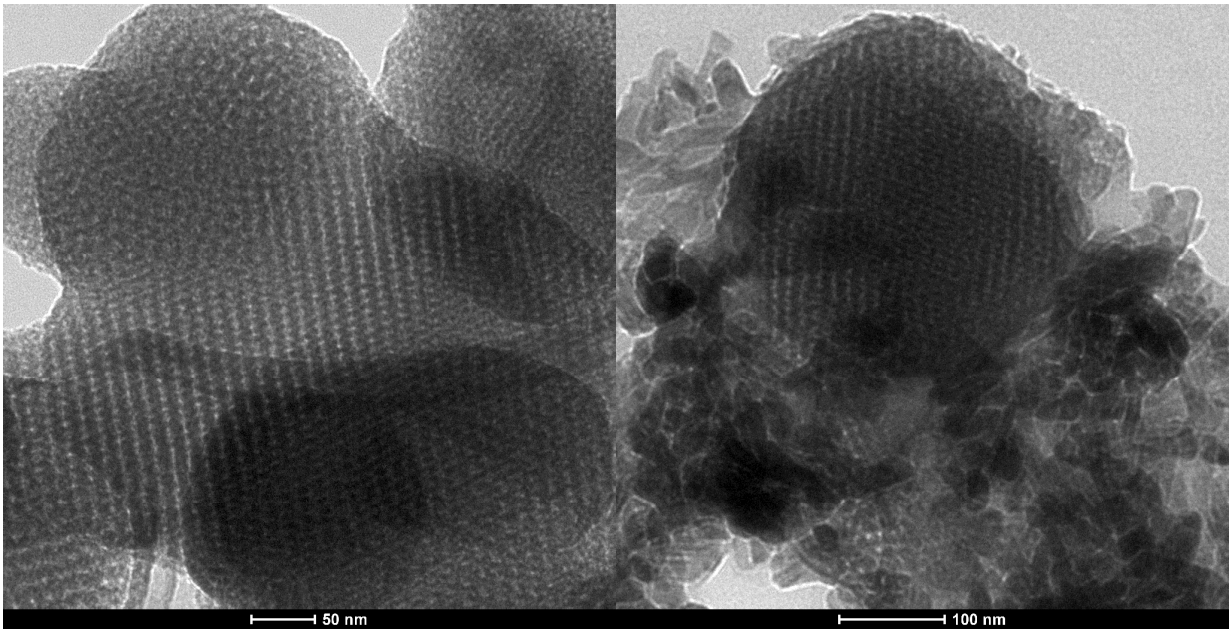

(a) **(b)**

Figure 2: Image of (a) SBA-16 sample with cubic structure and (b) HA/SBA-16 sample.

EDS spectrum of SBA-16 and HA/SBA-16 samples are presented (Figure 3). Qualitative elemental analysis shows the presence of silicon in the SBA-16 sample. Besides the presence of silicon in the HA/SBA-16 sample, calcium and phosphate ions are also present. This indicates the successful formation of calcium phosphate in the HA/SBA-16 structure.

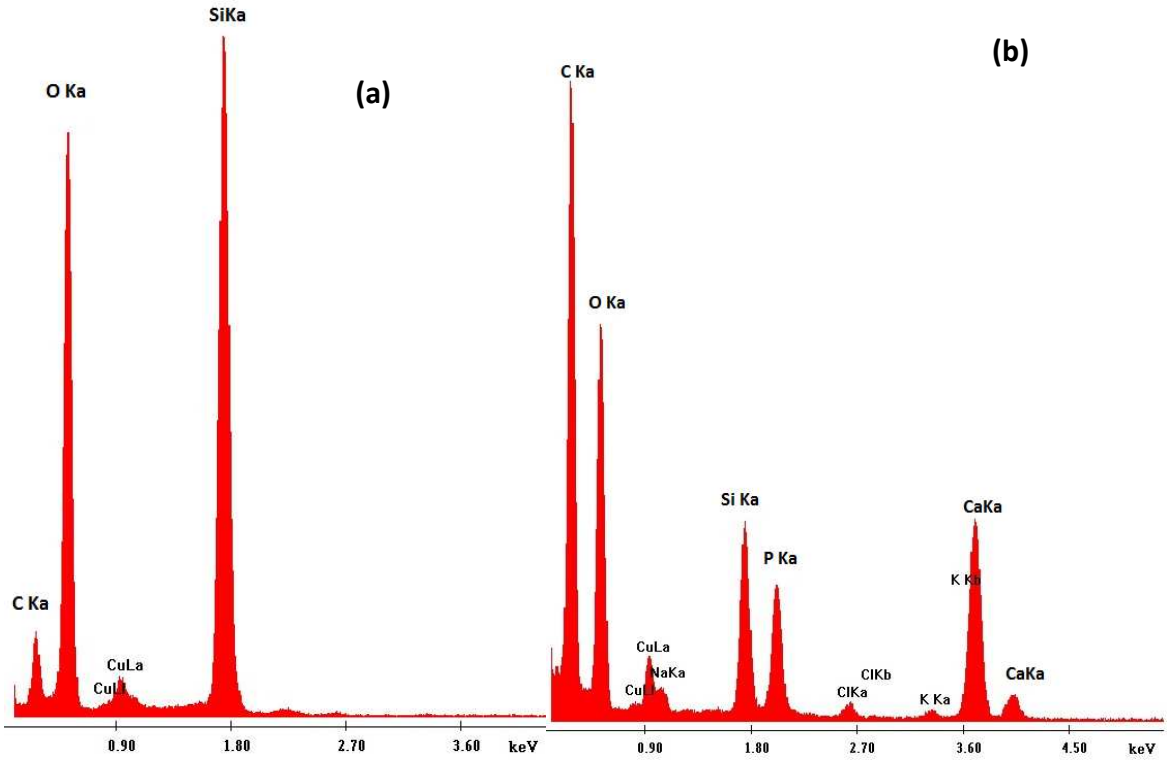

Figure 3: EDS of SBA-16 (a) e HA/SBA-16 (b) samples.

Thermogravimetry Analysis (TGA)

The thermal stability of the SBA-16 and HA/SBA-16 was determined by thermogravimetry. The TGA curves of all the systems are shown (Figure 4) and the results are summarized (Table 4). The SBA-16 shows an initial weight loss of 16.8% from 25° to 150°C, which is apparently due to the thermodesorption of physically adsorbed water. Above 150° and up to 800°C, no significant weight loss could be identified. In this temperature range, a small weight loss of approximately 2.3% was attributed to the decomposition of the residual F127 copolymer. As a result, the SBA-16 showed excellent thermal stability in the temperature range investigated. In case of the HA/SBA-16 sample, weight loss occurred in temperature range between 25° and 150°C, which can also be attributed to the thermodesorption of physically adsorbed water. The presence of the HA phase in the network causes a slightly hydrophobic character since the mass loss due to water molecules in

the pore interface, in the first region (20-150ºC), is much lower for the HA/SBA-16 sample (7.8%) when compared to silica-SBA-16 sample (16.8%). This can be ascribed to the amount of silanol groups on the surface of HA/SBA-16, which is less than in SBA-16 sample, and probably there are more siloxane linkages on the surface of HA/SBA-16, thereby reducing the hydrophilicity of this material. The second region showed weight loss between 150°- 800°C. The SBA-16 and HA/SBA-16 materials have adequate thermal stability for the proposed application, justifying the following biological assays.

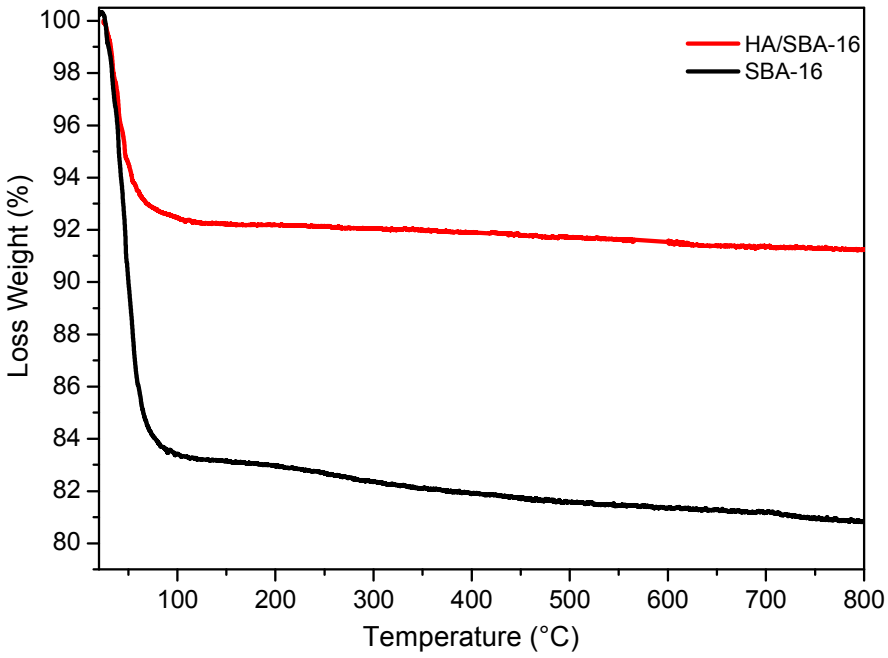

Figure 4: Curve of TG of SBA-16 and SBA-16-HA.

Table 5. Weight Loss.

Samples	Weight Loss (% w/w)	Weight Loss (% w/w)	Residue (%w/w)
	25-150 ºC	150-800 ºC	>800 ºC
SBA-16	16.8	2.3	80
HA/SBA-16	7.8	1.0	91

Isolation, Culture and Characterization of ASCs

The isolation of rat adipose tissue derived stem cells (ASCs) was successful. Isolated cells adhered to plastic and presented fibroblastic morphology, as depicted (Figure 5). Phenotypic profile was defined by flow cytometry, following the definition of Region of interest (ROI) according to size and internal complexity of the cell population and exclusion of cell debris (Figure 6A). Approximately 99% of the cells expressed CD90, 90% expressed CD73, 96% expressed CD54 and 90% of the cells expressed RT1A, a non-polymorphic determinant of rat MHC class I antigen. Additionally, cells lacked the expression of CD45, CD34, CD11b/c and anti-I-Ad/I-Ed, which are MHC class II alloantigens in rats (less than 5% of the cells expressed those markers). Representative histograms are shown (Figure 6B). ASCs were able to give rise to chondrocytes (Figure 6) and adipocytes (Figure 7) upon differentiation.

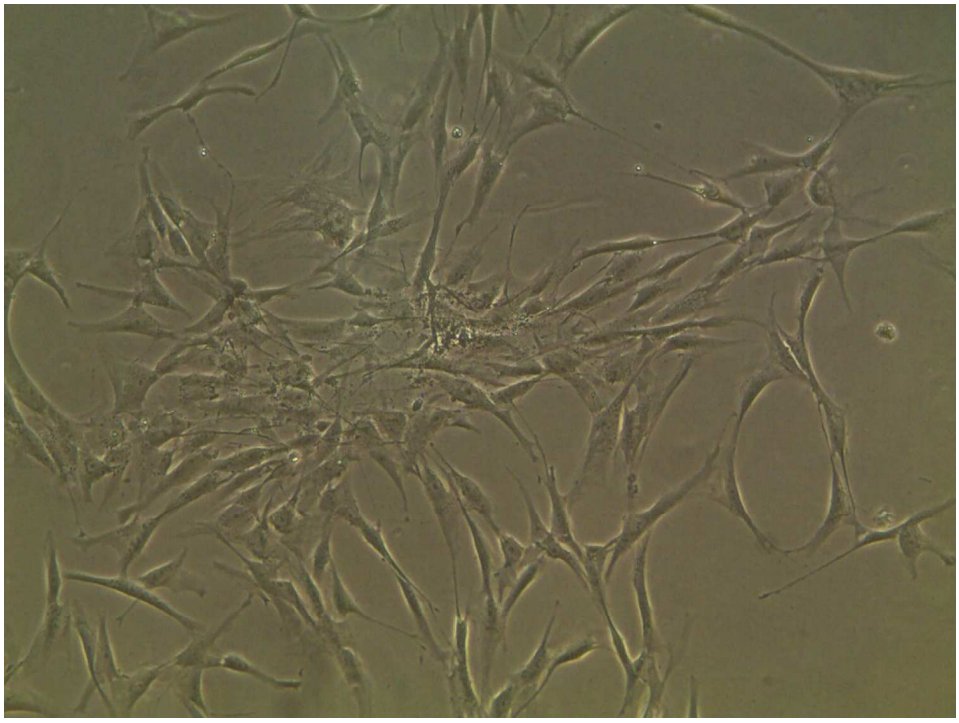

Figure 5: Morphology of Adipose Tissue-derived Stromal Cell cultures at passage 3 (20X).

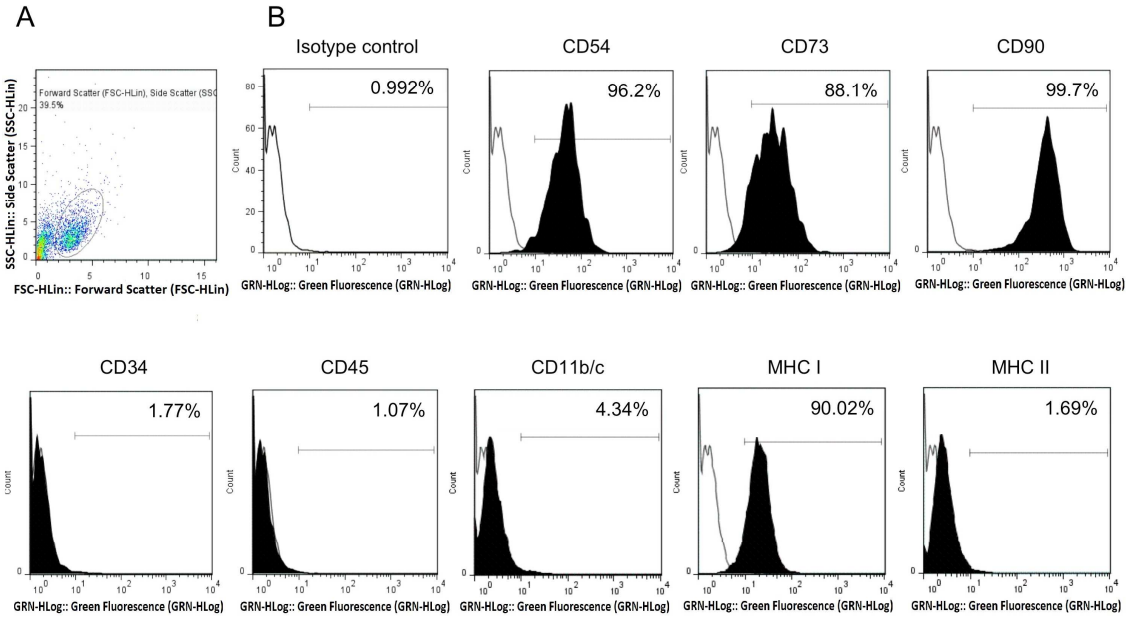

Figure 6: Characterization of ASCs according to mesenchymal stem cell markers. Phenotypic profile of isolated ASCs was assessed by flow cytometry. Flow cytometry dot plot represents cell

size and granularity (A). Histograms show staining profile of cell population stained with antibodies against indicated surface antigens (B). White peak indicates isotype-matched monoclonal antibody control and the black peak indicates positive stained cells.

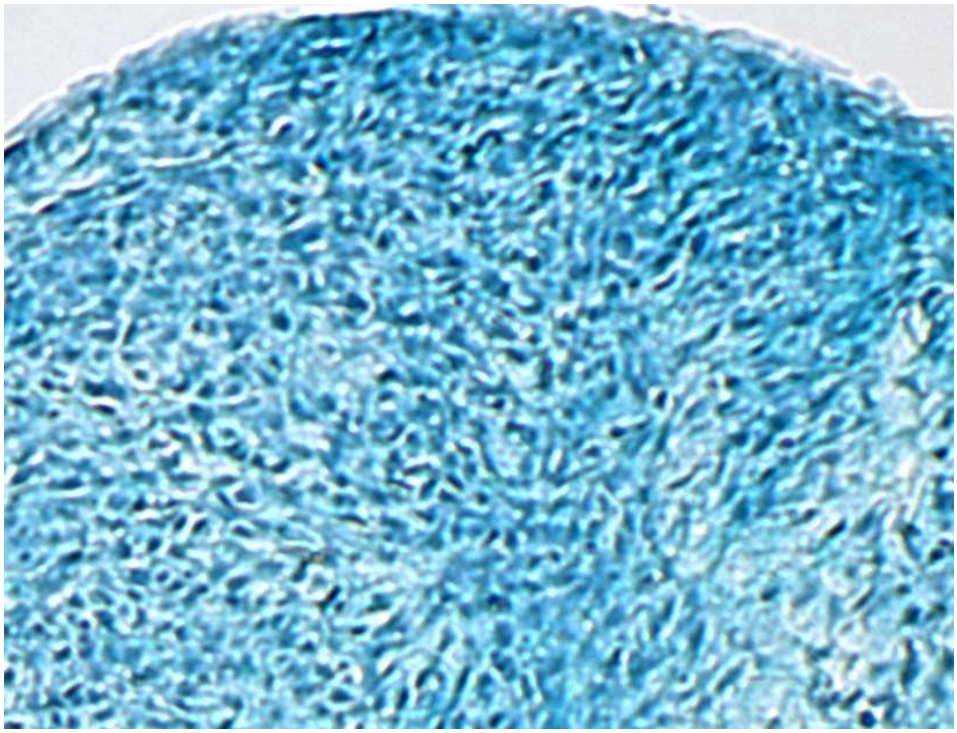

Figure 7: Chondrogenic differentiation capacity of ASCs. Three-dimensional pellet formed by ASCs was stained with Alcian Blue, and indicate the presence of proteoglycans deposited by ASC differentiated into functional chondrocytes. Magnification: 10x.

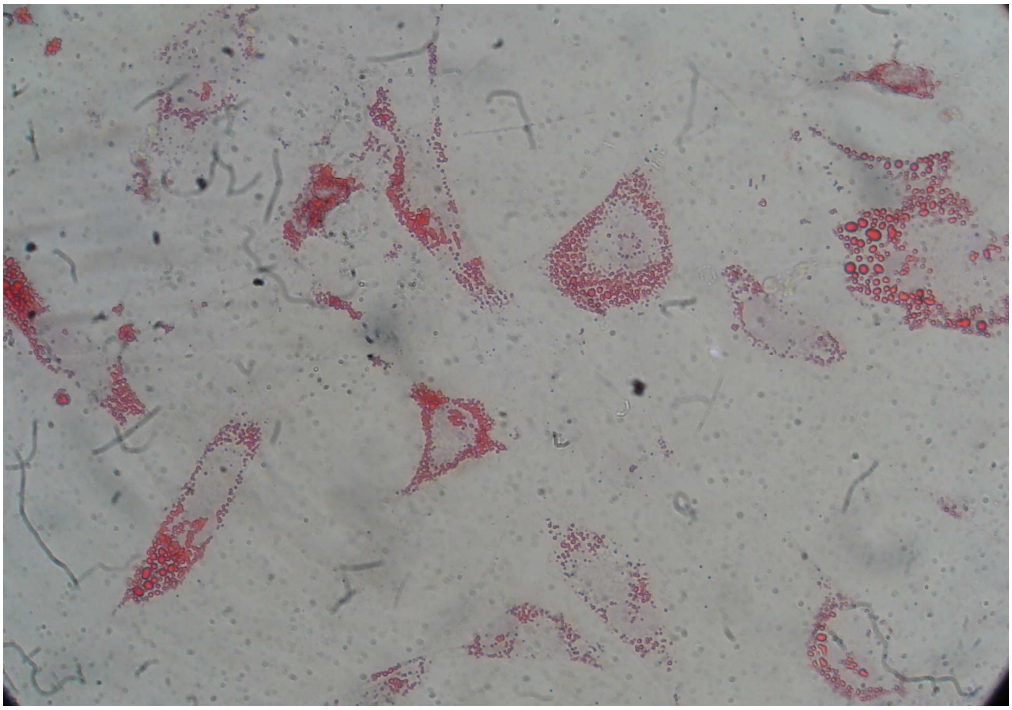

Figure 8: Adipogenic differentiation capacity of ASCs is evidentiated by the intracellular accumulation of lipid-rich vacuoles visualized by Oil Red staining. Magnification: 20x.

***In vitro* Cytotoxicity and Cell Proliferation During Differentiation**

SBA-16 and HA/SBA-16 cytotoxicity was assessed by the MTT assay and the results are showed (Figure 9). ASCs cultured in the presence of both biomaterials were capable of metabolizing MTT into formazan crystals, which demonstrated viability and proliferation. MSCs cultured in BM and OM in tissue culture polystyrene (TCPS) were viable and proliferated during the first two weeks, when cells reached confluency, stopped proliferating and decreased their viability. In contrast to TCPS groups, cells cultured in the presence of SBA-16 (Figure 9A) metabolized smaller amounts of MTT, indicative of minor cell viability or slower proliferation. Similar observations were made in the cells cultured in the presence of HA/SBA-16, even though at day 21 there was no difference between MTT metabolization in DMEM, as depicted (Figure 9B). Overall, MTT metabolization

was higher in cells cultured in the presence of HA/SBA-16 compared to SBA-16, indicating that HA presence increased cytocompatibility of the scaffold.

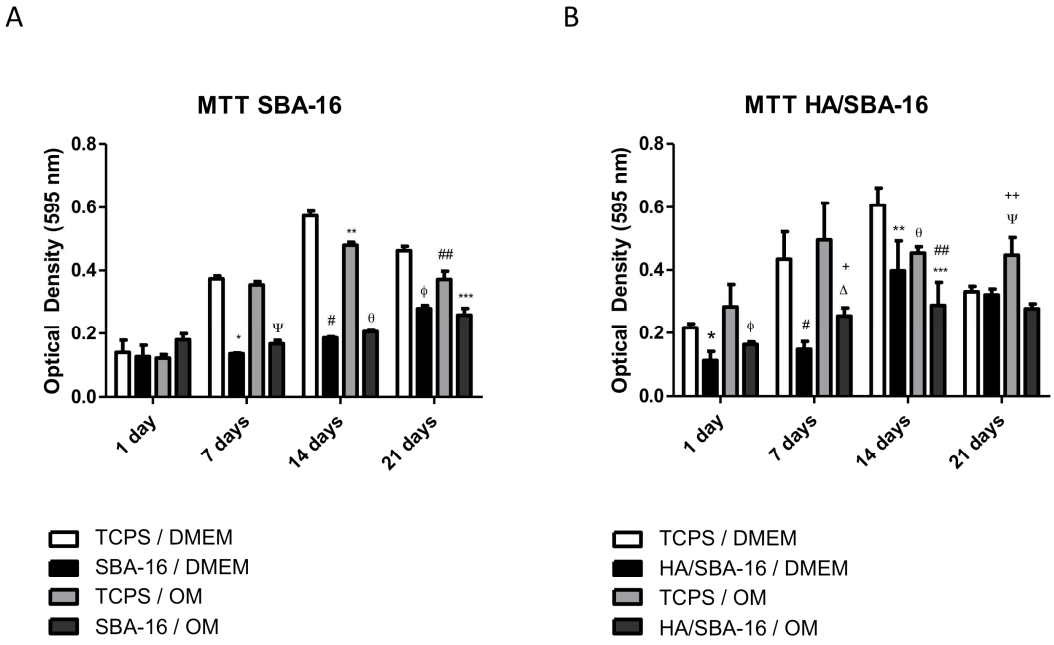

Figure 9: Citotoxicity of ASCs seeded on SBA-16 (A) and HA/SBA-16 (B) scaffolds as assessed by 3-(4,5-dimethylthiazol- 2-yl)-2,5-diphenyltetrazolium bromide assay during osteogenic differentiation. The results represent the viability and possible proliferation of ASC seeded on the different scaffolds as a function of time in basal medium (DMEM) or in Osteogenic medium (OM), in comparison to tissue culture polystyrene (TCPS). Data is represented as mean – standard deviation. In A: *p<0.05 compared to TCPS / DMEM at day 7. $^{\#}$p<0.05 compared to TCPS / DMEM at day 14. $^{\Phi}$p<0.05 compared to TCPS / DMEM at day 21. **p<0.05 compared to TCPS / DMEM at day 14. $^{\#\#}$p<0.05 compared to TCPS / DMEM at day 21. $^{\Psi}$p<0.05 compared to TCPS / OM at day 7. $^{\Theta}$p<0.05 compared to TCPS / OM at day 14. ***p<0.05 compared to TCPS / OM at day 21. In B: *p<0.05 compared to TCPS / DMEM at day 1. $^{\#}$p<0.05 compared to TCPS / DMEM at day 7. **p<0.05 compared to TCPS / DMEM at day 14. $^{\Psi}$p<0.05 compared to TCPS / DMEM

at day 21. $^{\Phi}p<0.05$ compared to TCPS / OM at day 1. $^{\Delta}p<0.05$ compared to HA/SBA-16 / DMEM at day 7. $^{+}p<0.05$ compared to TCPS / OM at day 7. ***$p<0.05$ compared to HA/SBA-16 / DMEM at day 14. $^{\#\#}p<0.05$ compared to TCPS / OM at day 14. $^{++}p<0.05$ compared to HA/SBA-16 / DMEM at day 21. $^{\Theta}p<0.05$ compared to TCPS / DMEM at day 14.

Alkalyne Phosphatase Production During Differentiation

ASCs cultured in the presence of SBA-16 presented smaller amounts of AP activity than control groups (Figure 10A), probably reflecting the smaller proliferation of those cells, as indicated in the MTT assay. On the other hand, ASCs cultured in the presence of HA/SBA-16 showed similar or higher levels of AP activity as cells in TCPS groups (Figure 10B). Those results allow suggesting that in contrast to SBA-16, HA/SBA-16 biomaterial induced an increase in AP production/activity of MSCs.

Gene Expression Assessment During Differentiation

The expression of osteogenic differentiation markers OC, OP and COL I was assessed by PCR at 21 days of ASC culture in BM and OM, as well as in TCPS or in the presence of SBA-16 and HA/SBA-16. OC and COL I mRNA were detected in ASC cultured in OM as well BM. OP, on the other hand, showed more specificity towards osteogenic differentiation, being expressed only by ASC cultured in OM and in ASC cultured in the presence of HA/SBA-16 in BM (Figure 11). This result corroborates the AP activity data, in which ASC cultured in BM and HA/SBA-16 had increased AP production.

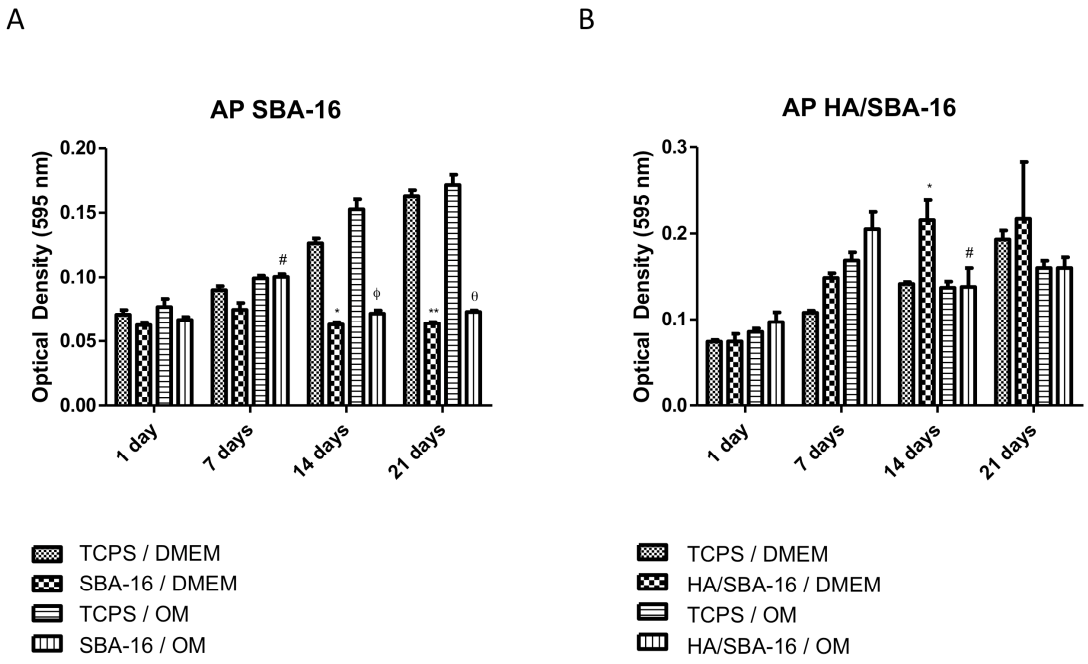

Figure 10: Alkaline Phosphatase (AP) assay of the ASC seeded on SBA-16 (A) and HA/SBA-16 (B) scaffolds as assessed by NBT-BCIP assay during osteogenic differentiation. The results are indicative of osteogenic differentiation of ASC seeded on the different scaffolds as a function of time in basal medium (DMEM) or in Osteogenic medium (OM), in comparison to tissue culture polystyrene (TCPS). In A: *$p<0.05$ compared to TCPS / DMEM at day 14. **$p<0.05$ compared to TCPS / DMEM at day 14. $^{\#}p<0.05$ compared to SBA-16 / DMEM at day 7. $^{\Phi}p<0.05$ compared to TCPS / OM at day 14. $^{\Theta}p<0.05$ compared to TCPS / OM at day 21. In B: *$p<0.05$ compared to TCPS / DMEM at day 14. $^{\#}p<0.05$ compared to HA/SBA-16 / DMEM at day 14.

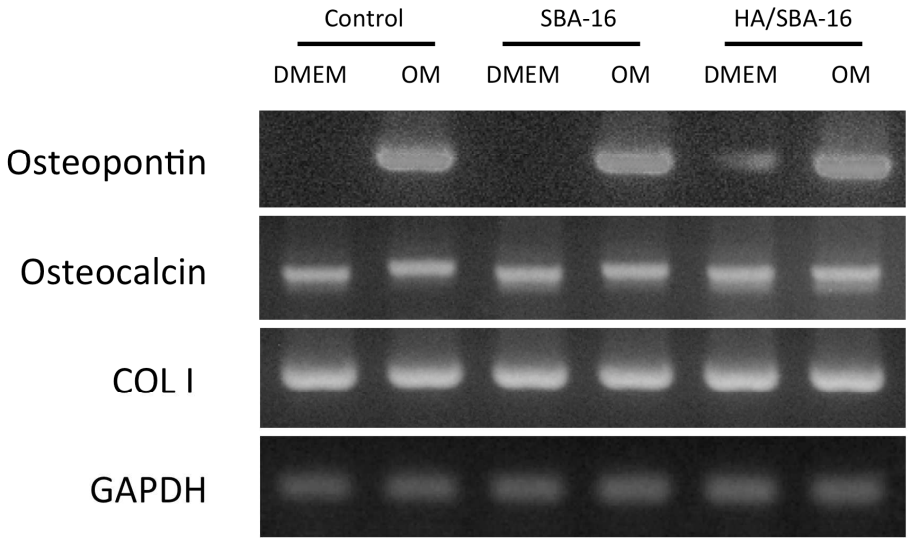

Figure 11: Reverse transcriptase–polymerase chain reaction analysis of OP, OC and collagen type I mRNA expression by ASCs grown on TCPS, SBA-16 and HA/SBA-16 over 21 days under basal or osteogenic media. GAPDH was assessed as the house-keeping gene.

ECM Mineralization

Finally, for functional evidence of osteogenic differentiation, the extracellular matrix mineralization staining protocol of Von Kossa was performed in cells cultured for 21 days in BM or OM, in TCPS or in the presence of SBA-16 and HA/SBA-16. Cells cultured in BM didn't mineralize ECM. However, ASCs cultured in OM or BM in the presence of HA/SBA-16 showed mineral accumulation in the ECM, compatible with osteogenic differentiation into functional osteoblasts (Figure 12). These results indicate that the cells cultured with SBA-16 and HA/SBA-16 scaffolds successfully differentiated into the osteogenic phenotype and that HA/SBA-16 functioned as an osteogenic differentiation induction component in the system.

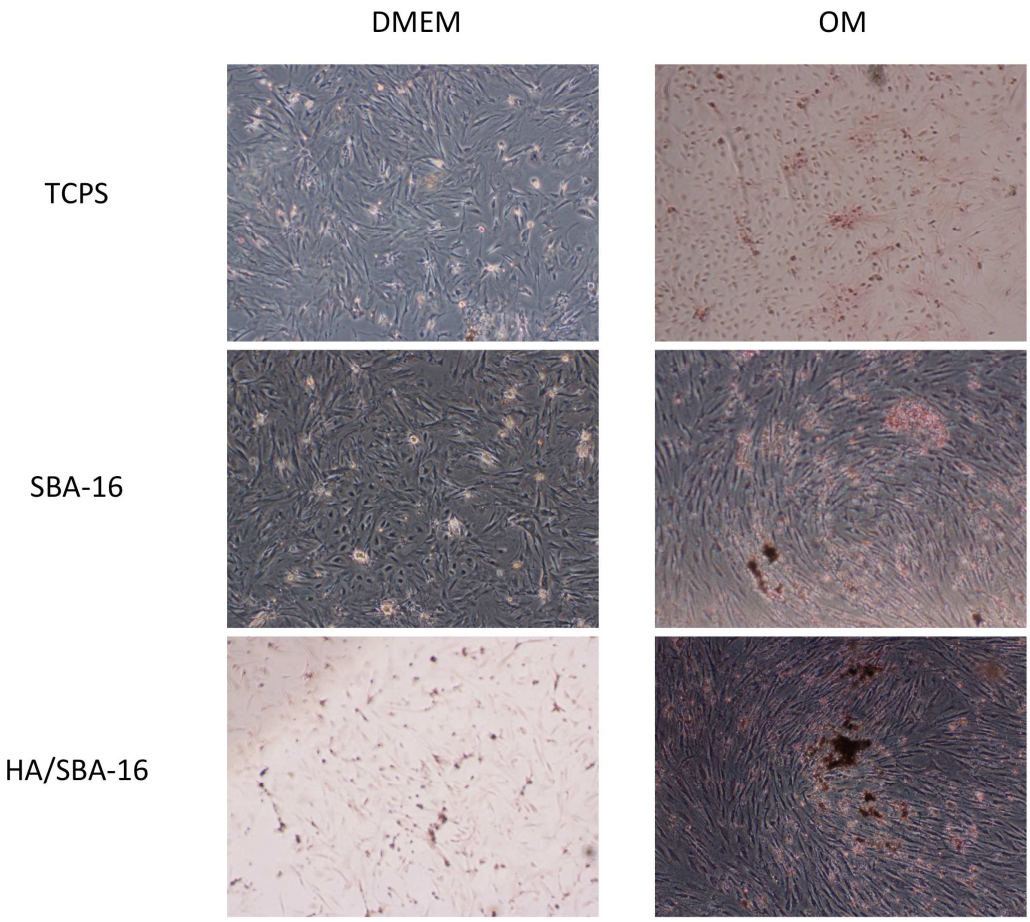

Figure 12: Analysis of the osteogenic differentiation of ASC cultured in TCPS, SBA-16 and HA/SBA-16 as assessed by Von Kossa staining during osteogenic differentiation. The results are indicative of osteogenic differentiation of ASC seeded on the different scaffolds as a function of time in basal medium (DMEM) or in Osteogenic medium (OM), in comparison to tissue culture polystyrene (TCPS).

DISCUSSION

Large bone defects are common lesions associated with several clinical conditions, such as infection, skeletal abnormalities, osteoporosis, tumor resection and trauma[24]. Frequently, following the aforementioned conditions, bone regeneration process is compromised or ineffective in

promoting tissue reconstitution. Among available strategies, autologous bone grafting is considered gold standard treatment, providing histocompatible and nonimmunogenic tissue for bone reconstitution. Unfortunately, though, this strategy also presents important limitations, as it requires additional surgical procedures, which are expensive and render limited amounts of tissue[25]. The ideal source of tissue for large bone reconstitution should be nonimmunogenic, available in large quantities and do not promote patient morbidity.

In such context, tissue engineering constitutes an innovative strategy for treatment of large bone defects. As stated by Langer and Vacanti in 1993, tissue engineering requires the association of cells, scaffolds and signaling molecules[12]. The search for the ideal combination of those components is still an active area of investigation.

Adult stem cells, such as adipose-derived stem cells (ASCs) have been actively investigated for bone tissue engineering purposes (clinicaltrials.gov, NCT01532076). Similar to bone marrow, adipose tissue also provides easily isolated stem cells with multipotent differentiation potential. In addition, those cells present advantages regarding their minimally invasive obtention procedures, as well as high proliferation capacity *in vitro*[16]. Therefore, it is expected that this cell type may be used for *in vitro* experiments of biomaterials designed for bone tissue engineering application.

In the present study, we have shown that the cell population isolated from adipose tissue is indeed a population of mesenchymal stem cells, according to the parameters established by the Mesenchymal and Tissue Stem Cell Committee of the International Society for Cellular Therapy in 2006[26]. As stated in the aforementioned document, ASCs should adhere to plastic, present a specific phenotype as well as multipotent differentiation potential. Here we show that our cells present all of those characteristics: first of all, we isolated the cells according to their capacity to adhere to plastic; second, cells expressed expected markers, namely: CD54, CD73, CD90 and

RT1A; third of all, cells lacked the expression of other cell types, such as hematopoietic and macrophagic cell lines, which include CD11b/c, CD34, CD45 and I-Ad/I-Ed, indicating that the culture was not contaminated with those cells. Finally, we have shown that cells were able to differentiate into: i. adipocytes able to storage lipid-rich vacuoles, evidentiated by Oil-Red O; ii. Chondrocytes able to deposite proteoglycan and glycosaminoglycan in the ECM, as stained by Alcian Blue staining; and iii. Isolated ASCs were able to differentiate into osteoblasts and mineralize the ECM, composing a robust dataset that allows suggesting that we worked with an adipose-derived cell population enriched with functional mesenchymal stem cells.

Concurrently to the search of the ideal cell source for bone tissue engineering, several attempts have been made to achieve the best scaffold for this application. Silica-based bioactive materials are a kind of bioceramic material. Bioactive materials have high reactivity due to their outstanding values of surface area, porosity and presence of silanol groups. Inside physiological fluids that material leads to the crystallization of the apatite-phase, similar to the inorganic components of bones[27]. In addition, degradation ionic products of silica species have shown osteoinductive properties[28]. Composites obtained by nucleation and growth of inorganic phases like Hydroxyapatite together with bioceramics are a good alternative as biomaterial[14]. On the base on the growth of calcium phosphate nanoparticles within an organized silica structure (SBA-16) it was developed the HA/SBA-16. Xynos et al [28] have shown that bioactive glass dissolution products exert a genetic control over the osteoblast cell cycle and rapid expression of genes that regulate osteogenesis and the production of growth factors. Recent molecular biology studies have shown that critical concentrations of soluble Ca and Si ions released from the bioactive materials control the cell cycle of osteoprogenitor cells[29].

In the present study, we proposed to assess the potential of SBA-16 and HA/SBA-16 as

biomaterials for tissue engineering applications. Therefore, we evaluated the cytotoxicity of the materials as well as their influence over the osteogenic differentiation of ASCs. Since the average pore sizes of such compositions are not large enough for cell colonization, we decided to evaluate their biological effects when present in the cell culture system. Cytotoxicity was assessed using MTT assay. This method, first described in 1983 by Mossman et.al.[30] is based on the reduction of the lipophilic positive charged tetrazolium salt, which achieves cytoplasm and mitochondria by endocytosis and is reduced by mitochondrial dependent dehydrogenases and endosome/lysosome membranes reductases[31]. In the past years, cytotoxicity, cell viability, and proliferation of living cells have been studied using the MTT assay.

Even though this assay has been traditionally used to assess cell viability and proliferation, it has recently been described that MTT assay may not be adequate to assess cell viability in the presence of some materials with higher oxidation potential compared to MTT, such as silicon microparticles[32]. In the present work, two mesoporous silicon biomaterias SBA-16 and HA/SBA-16 are evaluated performing MTT assay because they constitute completely oxidized materials and therefore are compatible with the assay.

According to the obtained data, both SBA-16 and HA/SBA-16 are compatible with ASCs, even though the cells proliferate less in their presence, which could explain the smaller MTT metabolization rates. Importantly, at no time the MTT metabolization rates of ASCs cultured in the presence of the biomaterials here tested were smaller than day 1, indicating that the cells did not die during this period, but probably proliferated at a smaller rate. This could be further evaluated, even though morphology analysis and the differentiation assays also corroborated the viability of the cells. If the cells died during those assays, no reliable information would be acquired which is not the case.

In addition to viability assay, cells cultured in the presence of SBA-16 and HA/SBA-16 were tested according to different parameters to robustly confirm osteogenic differentiation, such as AP production, expression of OC, OP and COL I, in addition to ECM mineralization capacity. As expected, once cultured in OM, ASCs were able to give rise to a population of cells with increased AP production, OC, OP and COLI positive gene expression profile and with ECM mineralizing potential, all compatible and determinant of osteogenic differentiation.

Curiously, HA/SBA-16 was sufficient to induce the osteogenic differentiation of ASCs. It is known that HA is an osteoconductive and osteoinductive factor, and the fact that the combination of HA and SBA-16 was indeed beneficial for the viability and differentiation of ASCs, even when cultured in BM, was actually a confirmation of the validity and quality of the designed biomaterial.

CONCLUSIONS

In the present study, we reported on the synthesis of composites consisting of mesoporous silica SBA-16 and another composition consisting of hydroxyapatite nanocrystals grown within mesoporous silica, which has objective as biomaterials for tissue engineering applications. This synthesis produced more hydrophobic surfaces than did the original silica matrix. Two mesoporous silicon biomaterials SBA-16 and HA/SBA-16 were evaluated for any potential cytotoxicity of the materials as well as their influence over the osteogenic differentiation of human ASCs. The results presented indicate that the cells cultured with SBA-16 and HA/SBA-16 scaffolds were viable and successfully differentiated into the osteogenic phenotype and that HA/SBA-16 functioned as an osteogenic differentiation inductor. Overall, the present data provides new information on a novel biomaterial composition, which combines the several

features of mesoporous silica with the biocompatible and biomimetic component HA. This dataset constitutes, therefore, an essential start point for further studies of this biomaterial *in vivo* and *in vitro*, when associated with biomolecules and used as a drug delivery system that may be applied to prevent graft infection and further accelerate engraftment and mineralization.

ACKNOWLEDGMENTS: This work was supported by funding from CAPES, CNPq, and FAPEMIG. Experiments and analyses involving electron microscopy were performed in the Microscopy Center of the Federal University of Minas Gerais, Belo Horizonte, Brazil (http://www.microscopia.ufmg.br).

REFERENCES

1 S. M. Best, a. E. Porter, E. S. Thian and J. Huang, *J. Eur. Ceram. Soc.*, 2008, **28**, 1319–1327.

2 D. Arcos and M. Vallet-Regí, *Acta Mater.*, 2013, **61**, 890–911.

3 P. D. D. C. and P. D. Y. L. Xueli Cheng, *ChemPhisChem*, 2012, **13**, 2392–2404.

4 D. Zhao, *Science (80-.).*, 1998, **279**, 548–552.

5 D. Zhao, Q. Huo, J. Feng, B. F. Chmelka and G. D. Stucky, *J. Am. Chem. Soc.*, 1998, **7863**, 6024–6036.

6 G. F. Andrade, D. C. F. Soares, R. G. dos Santos and E. M. B. Sousa, *Microporous Mesoporous Mater.*, 2013, **168**, 102–110.

7 Y. Hu, Z. Zhi, Q. Zhao, C. Wu, P. Zhao, H. Jiang, T. Jiang and S. Wang, *Microporous Mesoporous Mater.*, 2012, **147**, 94–101.

8 L. L. Hench, *J. Am. Ceram. Soc.*, 1991, **74**, 1487–1510.

9 I. D. X. & J. M. P. Larry L. Hench, *J. Biomater. Sci. Polym. Ed.*, 2004, **15**, 543–562.

10 G. F. Andrade, V. S. Gomide, A. C. da Silva Júnior, A. M. Goes and E. M. B. de Sousa, *J. Mater. Sci. Mater. Med.*, 2014, **25**, 2527–40.

11 P. Valerio, M. M. Pereira, A. M. Goes and M. F. Leite, *Biomaterials*, 2004, **25**, 2941–8.

12 R. Langer and J. P. Vacanti, *Science (80-.).*, 1993, **260**, 920–926.

13 O. C. Gobin, Université Laval, 2006.

14 A. Díaz, T. López, J. Manjarrez, E. Basaldella, J. M. Martínez-Blanes and J. a Odriozola, *Acta Biomater.*, 2006, **2**, 173–9.

15 A. C. C. de Paula, A. A. C. Zonari, T. M. D. M. Martins, S. Novikoff, A. R. P. da Silva, V. M. Correlo, R. L. Reis, D. A. Gomes and A. M. Goes, *Tissue Eng. Part A*, 2012, **19**, 121019095234000.

16 P. a Zuk, M. Zhu, H. Mizuno, J. Huang, J. W. Futrell, a J. Katz, P. Benhaim, H. P. Lorenz and M. H. Hedrick, *Tissue Eng.*, 2001, **7**, 211–28.

17 P. H. Carvalho, A. Paula, F. Daibert, B. S. Monteiro, B. S. Okano, J. Lott, D. Nunes, L. Silva, C. Favarato, V. G. Pereira, L. Eugênio, F. Augusto, R. Junqueira and D. Carlo, *Arq Bras Cardiol. 2013 Jan*, 2013, **100**, 82–89.

18 J. L. Carvalho, V. B. a Braga, M. B. Melo, A. C. D. a Campos, M. S. Oliveira, D. a Gomes, A. J. Ferreira, R. a S. Santos and A. M. Goes, *J. Cell. Mol. Med.*, 2013, **XX**, 1–9.

19 Y. Kimata, Y. I. Kimata, Y. Shimizu, H. Abe, I. C. Farcasanu, M. Takeuchi, M. D. Rose and K. Kohno, *Mol. Biol. Cell*, 2003, **14**, 2559–2569.

20 T. M. D. M. Martins, A. C. C. de Paula, D. A. Gomes and A. M. Goes, *Stem Cell Rev. Reports*, 2014, **10**, 697–711.

21 M. Berridge and A. Tan, *Arch. Biochem. Biophys.*, 1993, **303**, 474–482.

22 A. Sousa, K. C. Souza and E. M. B. Sousa, *Acta Biomater.*, 2008, **4**, 671–9.

23 X. Shi, Y. Wang, K. Wei, L. Ren and C. Lai, *J. Mater. Sci. Mater. Med.*, 2008, **19**, 2933–2940.

24 A. C. C. de Paula, A. A. C. Zonari, T. M. D. M. Martins, S. Novikoff, A. R. P. da Silva, V. M. Correlo, R. L. Reis, D. A. Gomes and A. M. Goes, *Tissue Eng. Part A*, 2012, **19**, 277–289.

25 T. a St John, A. R. Vaccaro, A. P. Sah, M. Schaefer, S. C. Berta, T. Albert and A. Hilibrand, *Am. J. Orthop. (Belle Mead. NJ).*, 2003, **32**, 18–23.

26 K. L.-C. M Dominici, *Cytotherapy*, 2006, **8**, 315–317.

27 D. Arcos and M. Vallet-Regí, *Acta Biomater.*, 2010, **6**, 2874–88.

28 I. D. Xynos, a J. Edgar, L. D. Buttery, L. L. Hench and J. M. Polak, *Biochem. Biophys. Res. Commun.*, 2000, **276**, 461–5.

29 L. L. Hench, J. M. Polak, I. D. Xynos and L. D. K. Buttery, *Mater. Res. Innov.*, 2000, **3**, 313–323.

30 T. Mosmann, *J. Immunol. Methods*, 1983, **65**, 55–63.

31 H. D.-L.-P. Matthieu Fisichella, *Toxicol. In Vitro*, 2009, **23**, 697–703.

32 H. S.-P. Timo Laaksonen, *Chem. Res. Toxicol.*, 2007, **20**, 1913–1918.